Modeling and Measurement of Vesicle Pools at the Cone Ribbon Synapse: Changes in Release Probability Are Solely Responsible for Voltage-Dependent Changes in Release

WALLACE B. THORESON,[1,2]* MATTHEW J. VAN HOOK,[1] CAITLYN PARMELEE,[3] AND CARINA CURTO[3,4]

[1]*Truhlsen Eye Institute, Department of Ophthalmology and Visual Sciences, University of Nebraska Medical Center, Omaha, Nebraska*
[2]*Department of Pharmacology and Experimental Neuroscience, University of Nebraska Medical Center, Omaha, Nebraska*
[3]*Department of Mathematics, University of Nebraska, Lincoln, Nebraska*
[4]*Department of Mathematics, Pennsylvania State University, State College, Pennsylvania*

KEY WORDS vesicle pools; ribbon synapse; cone photoreceptor; modeling

ABSTRACT Postsynaptic responses are a product of quantal amplitude (Q), size of the releasable vesicle pool (N), and release probability (P). Voltage-dependent changes in presynaptic Ca^{2+} entry alter postsynaptic responses primarily by changing P but have also been shown to influence N. With simultaneous whole cell recordings from cone photoreceptors and horizontal cells in tiger salamander retinal slices, we measured N and P at cone ribbon synapses by using a train of depolarizing pulses to stimulate release and deplete the pool. We developed an analytical model that calculates the total pool size contributing to release under different stimulus conditions by taking into account the prior history of release and empirically determined properties of replenishment. The model provided a formula that calculates vesicle pool size from measurements of the initial postsynaptic response and limiting rate of release evoked by a train of pulses, the fraction of release sites available for replenishment, and the time constant for replenishment. Results of the model showed that weak and strong depolarizing stimuli evoked release with differing probabilities but the same size vesicle pool. Enhancing intraterminal Ca^{2+} spread by lowering Ca^{2+} buffering or applying BayK8644 did not increase PSCs evoked with strong test steps, showing there is a fixed upper limit to pool size. Together, these results suggest that light-evoked changes in cone membrane potential alter synaptic release solely by changing release probability. **Synapse 70:1–14, 2016.**

INTRODUCTION

Postsynaptic responses in neurons are a product of the number of vesicles available for release (N), the probability that those vesicles will be released (P), and the quantal postsynaptic impact of a single vesicle (Q) (del Castillo and Katz, 1954). While Q can be altered by changes in vesicle size, vesicle glutamate levels, and postsynaptic receptor composition, these are slow processes that do not contribute to rapid voltage-dependent changes in postsynaptic responses (Bartoletti and Thoreson, 2011; Ishikawa et al., 2002; Karunanithi et al., 2002; Wilson et al., 2005; see Ariel and Ryan, 2012 for review). Instead, voltage-dependent changes in postsynaptic response amplitude are typically due to Ca^{2+}-dependent changes in

Contract grant sponsor: NIH; Contract grant numbers: R01EY10542 (WBT) and F32EY023864 (MJVH); Contract grant sponsor: NSF; Contract grant numbers: DMS-1225666 (CC) and DMS-1537228 (CC); Contract grant sponsor: Senior Scientific Investigator Award from Research to Prevent Blindness (WBT).

*Corresponding author: Wallace B. Thoreson, Truhlsen Eye Institute University of Nebraska Medical Center, 4050 Durham Research Center I, Omaha, NE 68198-5840. E-mail: wbthores@unmc.edu

Received 8 July 2015; Revised 21 September 2015; Accepted 6 October 2015

DOI: 10.1002/syn.21871

Published online 6 November 2015 in Wiley Online Library (wileyonlinelibrary.com).

P. However, at a number of synapses, including ribbon synapses of hair cells, greater stimulation can also produce changes in *N* (Furukawa and Matsuura, 1978; Ruiz et al., 2011; Thanawala and Regehr, 2013).

Light responses of cone photoreceptors are transmitted to downstream neurons in the visual system at their synapses onto second-order horizontal cells (HCs) and bipolar cells. Release of synaptic vesicles from cones occurs at plate-like protein structures known as ribbons (Snellman et al., 2011). Light causes cones to hyperpolarize from a dark resting potential of −35–45 mV, thus reducing the activation of L-type Ca^{2+} currents (I_{Ca}) in cone terminals. Synaptic release and, thus, postsynaptic currents (PSCs) vary linearly with the amplitude of I_{Ca} (Witkovsky et al., 1997; Thoreson et al., 2003, 2004). At cone ribbon synapses, the size of the readily releasable pool (RRP) of vesicles evoked by strong depolarizing stimulation appears to match the number of vesicles that lie in contact with the plasma membrane along the bottom two rows of the ribbons (Bartoletti et al., 2010). In this study, we asked whether voltage-dependent changes in I_{Ca} alter synaptic release at the cone ribbon synapse solely by altering *P* or whether there are also changes in the size of the total vesicle pool available for release (*N*). For example, we thought it possible that with stronger stimulation, greater spread of Ca^{2+} up the ribbon and into surrounding cytoplasm might provide access to a larger pool of vesicles.

Standard approaches for determining *N* use a train of depolarizing pulses to empty the releasable pool while measuring the change in release (Christensen and Martin, 1970; Elmqvist and Quastel, 1965). After emptying the releasable pool, the release rate levels out and becomes limited by the rate of replenishment. After accounting for replenishment rate, the number of vesicles in the releasable pool can be determined from the cumulative increase in release over time (Sakaba et al., 2002; Schneggenburger et al., 1999, 2002) or from the decline in synaptic responses accompanying depletion of the pool (Elmqvist and Quastel, 1965). However, these methods only measure the size of the pool that was emptied during the stimulus train. If a train of weakly depolarizing stimuli does not empty the entire pool, then these methods can only measure the released fraction of the pool and not the total available pool size. This is likely to be the case at bipolar cell and cone ribbon synapses where maintained sub-maximal depolarization does not cause progressive depletion of the entire RRP but instead empties a fixed fraction of the RRP (Babai et al., 2010; Oesch and Diamond, 2011). In addition, the fraction of release sites available for replenishment can be regulated by intracellular Ca^{2+} levels and can, therefore, vary with stimulation strength (Gomis et al., 1999; Van Hook et al., 2014). We developed an analytical model to measure the total vesicle pool available for release even when using weak stimuli that do not empty the entire pool. The model also incorporates empirically determined properties of replenishment. From the model, we derived a formula that calculates pool size from measurements of the initial postsynaptic response and the limiting rate of release evoked by a train of pulses, the fraction of release sites available for fast replenishment, and the time constant for replenishment. The model, which allowed both pool size and release probability to vary, showed that weak and strong stimulation emptied vesicles from a total available pool of the same size at cone ribbon synapses. Changes in cone membrane potential are, therefore, encoded into postsynaptic responses solely by changes in release probability. This in turn suggests that, like bipolar cell ribbon synapses (Oesch and Diamond, 2011), changes in luminance are encoded at cone ribbon synapses by changes in the occupancy state of a readily releasable pool of vesicles. The total vesicle pool released by sustained strong stimulation was not limited to the RRP but was instead similar in size to the number of vesicles attached to the entire ribbon. This is similar to findings at bipolar cell ribbon synapses (von Gersdorff et al. 1996) and supports the idea that the rate-limiting step during sustained release is vesicle attachment to the ribbon (Van Hook et al., 2014). The ability of this analytical model to calculate pool size and release probability under widely varying conditions of vesicle pool occupancy provides useful advantages for calculating synaptic vesicle pool size.

MATERIALS AND METHODS

Animals

Experiments were performed using retinas of aquatic tiger salamanders (*Ambystoma tigrinum*; Charles Sullivan, Nashville, TN) of both sexes (18–25 cm in length). Care and handling protocols were approved by the Institutional Animal Care and Use Committee at the University of Nebraska Medical Center. Animals were housed on a 12-h light/dark cycle at 4–8°C. One to 2 h after the beginning of the dark cycle, animals were decapitated, quickly pithed, and enucleated.

Retinal slices

Details of the retinal slice preparation and whole cell recording are described elsewhere (Van Hook and Thoreson, 2013). Briefly, the anterior segment of the eye, including the lens, was removed, and the resulting eyecup was cut into quarters. One or two pieces were placed vitreal side down on a nitrocellulose membrane (5 × 10 mm; type AAWP, 0.8-μm pores; Millipore, Bedford, MA). The filter paper with pieces

of eyecup was submerged in cold amphibian saline, and the sclera was gently peeled away, leaving the retina adhering to the membrane. The retina was then cut into 125-μm slices using a razor blade tissue slicer (Stoelting, Wood Dale, IL), and slices were rotated 90° to view the retinal layers and anchored in the recording chamber by embedding the ends of the filter paper in vacuum grease. Slices were prepared under fiber optic illumination.

Patch clamp electrophysiology

Recordings were performed on an upright fixed-stage microscope (E600FN; Nikon, Tokyo, Japan) equipped with a 60× water-immersion objective. Slices were superfused at ~1 mL/min with an oxygenated amphibian saline solution containing the following (in m*M*): 116 NaCl, 2.5 KCl, 1.8 $CaCl_2$; 0.5 $MgCl_2$; 5 glucose, and 10 HEPES. The pH was adjusted to 7.8 with NaOH. Osmolarity was measured with a vapor pressure osmometer (Wescor, Logan, UT) and adjusted to 240–245 mOsm. Unless otherwise specified, chemicals were obtained from Sigma Chemicals (St. Louis, MO).

Patch pipettes were pulled from borosilicate glass (1.2 mm OD, 0.9 mm ID, with an internal filament; World Precision Instruments, Sarasota, FL) using a PC-10 vertical pipette puller (Narishige, East Meadow, NY) and had resistances of 15–20 MΩ. The standard pipette solution for cones contained (in m*M*): 90 CsOH, 50 gluconic acid, 40 glutamic acid, 10 TEA-Cl, 3.5 NaCl, 1 $CaCl_2$, 1 $MgCl_2$, 9.4 ATP-Mg, 0.5 GTP-Na, 10 HEPES, and 5 EGTA. The pH was adjusted to 7.2, and the osmolarity was adjusted to 235–240 with CsOH. In some experiments, indicated in the Results, we reduced Ca^{2+} buffering by using the following cone pipette solution (in m*M*): 90 CsOH, 50 gluconic acid, 40 glutamic acid, 10 TEA-Cl, 3.5 NaCl, 2 $MgCl_2$, 9.4 ATP-Mg, 0.5 GTP-Na, 10 HEPES, and 0.05 EGTA. With 40 m*M* glutamate in the cone pipette solution, PSC amplitude at cone to HC synapses increases over the first 1–2 min after patch rupture but after that, remains stable for >15 min (Bartoletti and Thoreson, 2011). Our experiments were conducted during that time of stability when the quantal amplitude of mEPSCs was relatively constant. For recordings from HCs, the pipette solution was the same except that the glutamic acid was replaced with an additional 40 m*M* gluconic acid. Passive parameters in cone cells averaged membrane capacitance (C_m) = 79.9 ± 4.6 pF, membrane resistance (R_m) = 303 ± 15 MΩ, and series resistance (R_s) = 45.3 ± 1.1 MΩ (n = 35). Passive parameters in HCs were C_m = 46.4 ± 3.5 pF, R_m = 416 ± 90 MΩ, and R_s = 48.8 ± 3.6 MΩ (n = 16). Voltage values were corrected for a measured liquid junction potential of −9 mV but not for series resistance errors.

Whole-cell patch clamp recordings were made from HCs and cones under white-light illumination. Cells were targeted based on morphology and soma position and identity of horizontal cells was confirmed by physiological criteria and their responses to a flash of light (Van Hook and Thoreson, 2013). Cones were voltage clamped at −79 mV and horizontal cells were voltage clamped at −69 mV with a Multiclamp 700A amplifier (Molecular Devices, Sunnyvale, CA). For paired recordings, we targeted cones and postsynaptic neurons positioned adjacent to one another in the slice. Signals were digitized at 10 kHz with a Digidata 1322A A:D/D:A interface (Molecular Devices) and low pass filtered with a cutoff of 2 kHz. Recordings were excluded if the cone access resistance exceeded 60 MΩ or changed dramatically over the course of the recording or if the cone holding current >200 pA.

To measure pool size, we used trains of depolarizing pulses that mimic the range of voltage values experienced by cones, from hyperpolarizing light responses to the depolarizing overshoot that sometimes follows light offset (25 ms pulses to −49, −39, −29, or −19 mV). Pool size was measured from the y-intercept of a straight line fit to the cumulative amplitude or charge transfer of the postsynaptic responses evoked from 1 to 2 s into the train (Sakaba et al., 2002). We adjusted the baseline to remove contributions from background synaptic inputs prior to the pulse train. We also assessed pool size using the approach of Elmqvist and Quastel (1965) in which PSC amplitude is plotted on the y-axis and cumulative PSC amplitude on the x-axis. The size of the RRP is estimated from the x-intercept of a line fit to the initial decline in EPSC amplitude. Release kinetics were measured from the fast time constant of a dual exponential function fit to the initial rise in PSC charge transfer during a depolarizing test pulse applied to the cone. The time course of replenishment was measured from the ratio of PSC amplitudes evoked by a pair of depolarizing pulses (100 ms steps to −19 or −39 mV) applied to the cone with interstimulus intervals ranging from 200 ms to 30 s.

RESULTS

Electrophysiological measurements of release

To measure the number of vesicles in the releasable pool at the cone synapse, we stimulated cones with a train of depolarizing test pulses while simultaneously recording PSCs in postsynaptic HCs. Figure 1 shows examples of cone-driven PSCs evoked in a HC by trains of pulses to −19 mV (Fig. 1A), −29 mV (Fig. 1B), −39 mV (Fig. 1C), and −49 mV (Fig. 1D) applied to a simultaneously voltage-clamped cone. Fully activating I_{Ca} with a strong test step to −19 mV (25 ms) evoked a PSC averaging −128.2 ± 10.9 pA (n = 13). An individual cone can contact a postsynaptic HC at

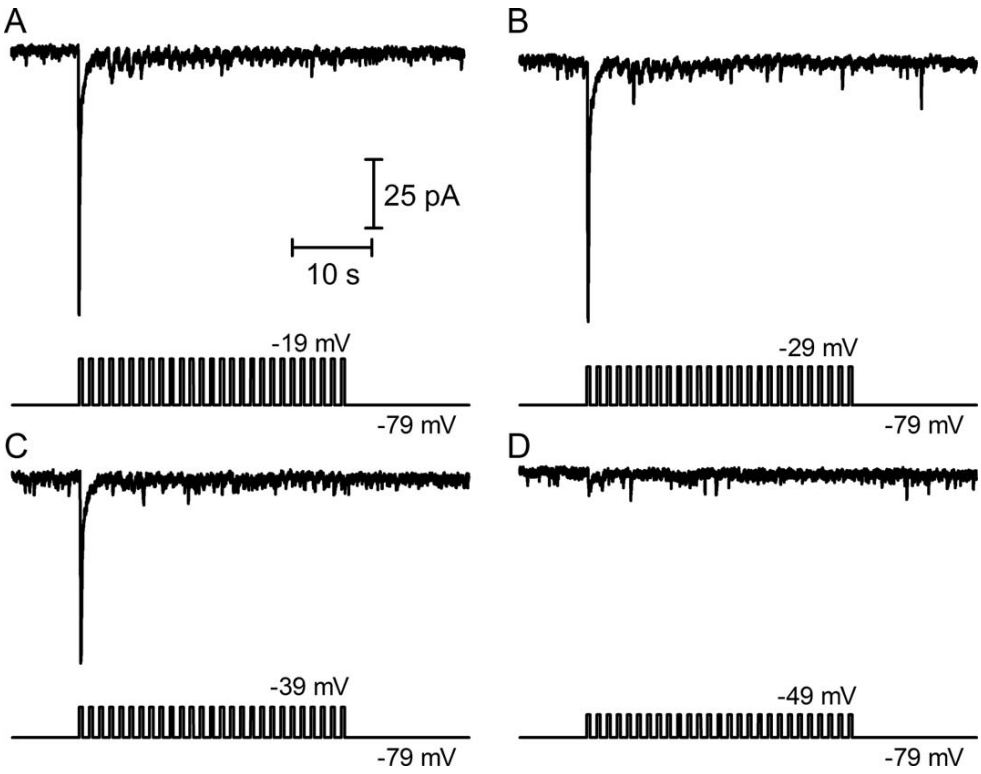

Fig. 1. Postsynaptic currents (PSCs) evoked in a horizontal cell by application of depolarizing pulse trains (25 ms, 13.3 Hz) to a simultaneously voltage-clamped presynaptic cone. Test pulse amplitudes were −19 (A), −29 (B), −39 (C), and −49 mV (D).

more than one ribbon. Previous work has shown that a single ribbon contributes an average of 46 pA to the peak amplitude of the HC PSC evoked by a strong test step applied to the cone (Bartoletti et al., 2010). Dividing the average peak PSC amplitude of 128 pA by 46 pA/ribbon yielded an average of 2.78 ribbon contacts in this sample of cone/HC pairs (Table I).

Application of a train of strong depolarizing pulses to the presynaptic cone quickly emptied the releasable pool of vesicles and, so, release soon attained a steady state where it increased at a linear rate limited by replenishment. Assuming the number of release sites available for replenishment remained constant, the size of the original vesicle pool can be estimated after subtracting the replenishment rate by fitting a straight line to the cumulative increase in release and projecting that line back to the *y*-intercept (Sakaba et al., 2002). The *y*-intercept of the cumulative increase in PSC amplitude during a train of depolarizing test pulses to −19 mV was -126.2 ± 7.0 pA (Fig. 2A). This is close to the amplitude of first PSC evoked during the train (−128.2 pA), consistent with a cumulative release probability of 0.98 during the first pulse, as found earlier (Bartoletti et al., 2010).

Cones can depolarize to around −20 mV during the overshoot following a bright light flash but to study membrane potentials that are more often encountered under physiological conditions, we measured pool sizes emptied by trains of depolarizing steps at less depolarized potentials of −29, −39, and −49 mV. Given some series resistance, the test step to −29 mV attained a potential somewhat above the dark resting potential, whereas −49 mV would mimic the response to a moderate light flash. The amount of release declined with use of weaker depolarizing test steps, resulting in smaller HC PSCs (Fig. 1). Along with the smaller PSCs evoked by weaker steps, the *y*-intercept of a straight line fit to the cumulative amplitude of PSCs evoked by trains of steps to −29 mV was smaller than the *y*-intercept observed with a train of steps to −19 mV (Fig. 2A). This shows that fewer vesicles were depleted by a train of pulses to −29 mV compared with the stronger train of pulses. The number of released vesicles declined still further when the test pulse amplitude was reduced to −39 mV (Fig. 2A). PSCs evoked by steps to −49 mV were too small for reliable measurement of cumulative PSC amplitude.

Elmqvist and Quastel (1965) measured pool size by plotting EPSC amplitude along the ordinate and the cumulative increase in EPSC amplitude along the abscissa. During a pulse train, the RRP is depleted to

TABLE I. Vesicle pool sizes predicted from the model under different experimental conditions

Experimental conditions	PSC amplitude (1^{st} pulse)	Predicted pool size (PSC amplitude)	Predicted pool size ratio (A_{-39}/A_{-19})	Average number of ribbon contacts (cone/HC)	RRP from charge transfer (vesicles/ribbon)	Total pool size from charge transfer (vesicles/ribbon)
$T = 50$ ms, $\Delta t = 25$ ms to -19, 5 m*M* EGTA	128.2 ± 10.9 pA ($n = 13$)	131.3 pA	1.0	2.79	17.1	64
$T = 50$ ms, $\Delta t = 25$ ms to -39, 5 m*M* EGTA	70.9 ± 7.4 pA	131.2 pA				
$T = 125$ ms, $\Delta t = 25$ ms to -19, 5 m*M* EGTA	135.5 ± 15.8 pA ($n = 6$)	136.9 pA	0.96	2.95	16.8	70
$T = 125$ ms, $\Delta t = 25$ ms to -39, 5 m*M* EGTA	71.3 ± 12.8 pA	131.2 pA				
$T = 50$ ms, $\Delta t = 25$ ms to -19, 0.05 m*M* EGTA	91.1 ± 18.2 pA ($n = 8$)	110.9 pA	1.02	1.98	18.2	80
$T = 50$ ms, $\Delta t = 25$ ms to -39, 0.05 m*M* EGTA	38.5 ± 9.5 pA	113.6 pA				

The first column summarizes the experimental conditions for each sample of cone/horizontal cell pairs. The second column shows the mean amplitude of PSCs evoked by the first step applied to the pulse train (either −19 or −39 mV). The third column shows the PSC amplitude that would be evoked by release of the entire RRP as predicted by the model. The fourth column shows the ratio of pool sizes predicted by the model for weak (−39 mV) and strong (−19 mV) stimuli. The fifth column shows the average number of ribbon contacts for each sample of cells calculated by dividing the amplitude of the PSC evoked by a pulse to −19 mV by the average amplitude contributed by a single ribbon (46 pA/ribbon). The sixth column shows the RRP per ribbon calculated from the amplitude of the fast component of PSC charge transfer evoked by a step to −19 mV applied to the cone. For this calculation, we used a single vesicle charge transfer of 15.5 fC (Cadetti et al., 2008). The final column shows the entire pool size calculated from the *y*-intercept value of the cumulative increase in charge transfer plotted against time during a train of pulses to −19 mV. See text for further details.

a steady state level and, so, the size of the RRP can be estimated from the *x*-intercept of a line fit to the initial decline in EPSC amplitude. At the photoreceptor synapse, PSCs declined almost to zero by the second test pulse and so, similar to the data described earlier, pool sizes given by this approach are similar in size to the first EPSC evoked by each stimulus: −39 mV, 80 pA; −29 mV, 105 pA; and −19 mV, 132 pA (Fig. 2B).

There is minimal cross-desensitization or saturation between quanta at the cone-HC synapse (Cadetti et al., 2008; Pang et al., 2008) and, so, glutamate release quantified from PSC charge transfer linearly tracks release measured presynaptically using capacitance techniques (Rabl et al., 2005). PSCs can thus be treated as a linear sum of individual mEPSCs (Cadetti et al., 2005, 2008), allowing them to be used to measure the total number of released vesicles. As illustrated by the example in Figure 3A, the increase in PSC charge transfer evoked by the first step in the pulse train could be fit with a dual exponential function (dashed line, Fig. 3A), reflecting fast and slow components of release. Consistent with earlier results (Bartoletti et al., 2010), we found that the amplitude of the fast component averaged 738 ± 1.8 fC. Given a single vesicle amplitude of 15.5 fC/vesicle (Cadetti et al., 2008) and an average of 2.78 ribbon contacts per cone/HC pair, this suggests that the fast component that reflects release of the RRP arises from release of 17.1 vesicles/ribbon. This matches the number of vesicles that contact the plasma membrane along the bottom two rows of the ribbon (Bartoletti et al., 2010).

When integrating the entire train of PSCs, the cumulative increase in charge transfer flattened out about 1 s into the pulse train began to rise at a steady linear rate after the initial double exponential rise. As with cumulative amplitude plots, we fit a straight line to the linear increase in charge transfer between 1 and 2 s. With a train of 25 ms pulses to −19 mV (50 ms intervals), the maximum available pool size suggested by the y intercept of this straight line fit averaged −2773 ± 87.4 fC (179 vesicles) or 64 vesicles/ribbon. This is greater than the number of vesicles in the RRP determined from the size of the initial fast component to charge transfer suggesting that additional vesicles on the ribbon are released during the pulse train. Similar to cumulative amplitude plots, the number of vesicles depleted by the pulse train declined progressively as the amplitude of test pulses was reduced from −19 to −29, −39, and −49 mV (Fig. 3B,D).

To test whether glutamate receptor desensitization might contribute to these voltage-dependent changes in pool size, we blocked AMPA receptor desensitization with cyclothiazide (CTZ, 0.1 m*M*). The PSC evoked by the first test pulse in a train was increased

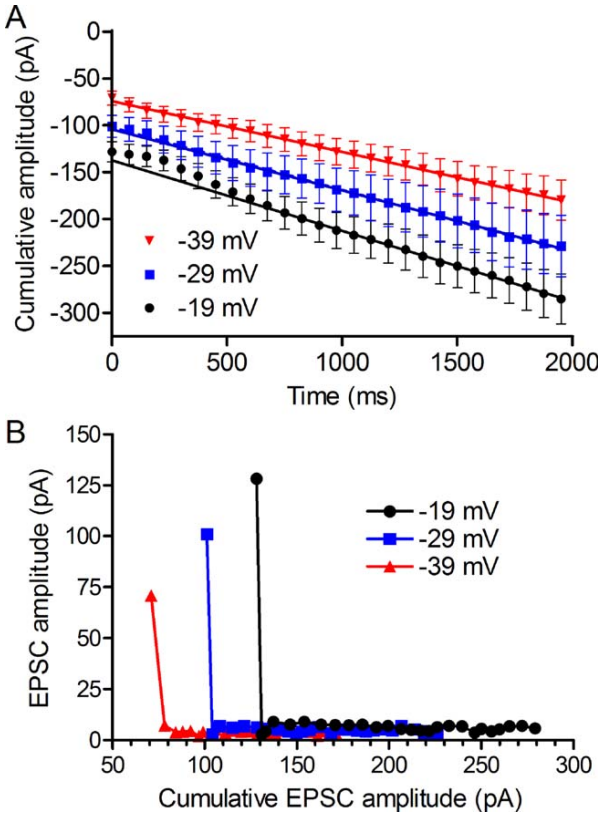

Fig. 2. A: Cumulative amplitude of PSCs evoked by trains of pulses to −19, −29, and −39 mV ($N = 13$ cone/horizontal cell pairs). The amplitude of the releasable pool was estimated from the y-intercept of straight lines fit to the final 1.2 s of the 2-s pulse train. B: Pool size measured by plotting EPSC amplitude against the cumulative increase in EPSC amplitude. In this approach, pool size can be estimated from the x-intercept of a line fit to the initial decline in EPSC amplitude. EPSCs declined almost to zero by the second test pulse, and, so, pool sizes given by this approach were similar to the size of the first EPSC evoked by each stimulus: −39 mV, 80 pA; −29 mV, 105 pA; and −19 mV, 132 pA.

considerably by application of CTZ, averaging 395.2 ± 53.1 pA when evoked by a step to −19 and 307.7 ± 41.7 pA when evoked by a step to −39 mV ($n = 9$; Fig. 3C). However, the relative changes in y-intercept values observed with strong and weak steps did not change. Using the first approach for measuring pool size, the y-intercept of the cumulative increase in charge transfer evoked by a train of pulses to −39 mV averaged 63.0 ± 6.4% of the y-intercept value obtained from a train of pulses to −19 mV. This was similar to control conditions where the y-intercept evoked by a train of pulses to −39 mV averaged 59.3 ± 4.2% ($n = 13$) of the y-intercept measured with trains of pulses to −19 mV.

The aforementioned results show that with weak, submaximal depolarization of the presynaptic cone, a smaller pool of vesicles is depleted. But are the decreases in pool size observed with weaker steps entirely due to reduced release probability stimulating

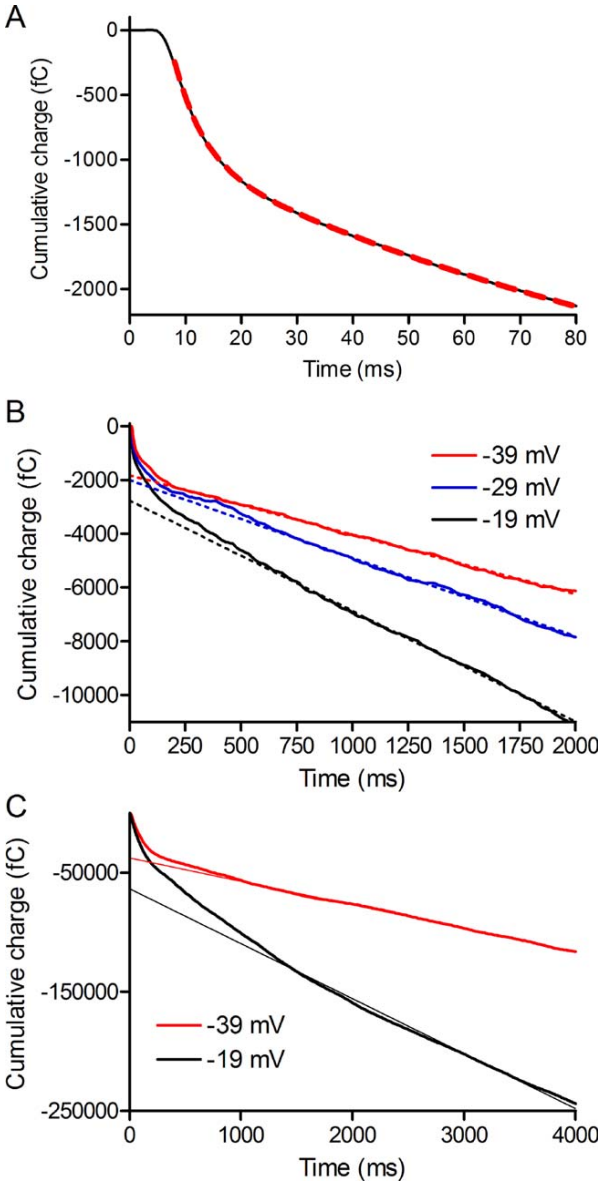

Fig. 3. A: Average PSC charge transfer in horizontal cells evoked by a step to −19 mV applied to cones ($N = 13$; same data as Fig. 2). The rise in charge transfer was fit with a double exponential function (dashed red line): $\tau_{fast} = 5.2$ ms, amplitude = 865 fC; $\tau_{slow} = 119$ ms, amplitude = 2665 fC. B: Pool size measurements from cumulative charge transfer during pulse trains (25 ms pulses, 13.3 Hz; −19, −29, and −39 mV). The amplitude of the releasable pool was estimated from the y-intercept of straight lines fit to the final 1.2 s of the 2 s pulse train. C: Pool size measurements from cumulative charge transfer during pulse trains measured in the presence of 0.1 mM cyclothiazide used to block AMPA receptor desensitization (25 ms pulses, 13.3 Hz; −19 and −39 mV). The amplitude of the releasable pool was estimated from the y-intercept of straight lines fit between 1.1 and 4 s during the pulse train.

release of fewer vesicles from a single large fixed pool? Or is there also a change in the total number of vesicles available for release? We addressed these questions with additional experiments and modeling.

Enhancement of Ca^{2+} spread

Stronger depolarizing voltage steps should cause a greater spread of Ca^{2+}, and this could potentially expand pool size by allowing access to a larger pool of vesicles. Experiments described earlier were performed using 5 m*M* EGTA as the intracellular Ca^{2+} buffer in the patch pipette solution. However, recent studies have shown that cones possess an endogenous Ca^{2+} buffering capacity equivalent to only ~0.05 m*M* EGTA (Van Hook and Thoreson, 2014). With 0.05 m*M* EGTA as the principal intracellular Ca^{2+} buffer in the cone patch pipette solution, the amplitude of PSCs evoked in HCs by a test pulse to −19 mV applied to cones averaged 91.1 ± 18.2 pA ($n = 8$; Fig. 4A). There is variability among cone–HC pairs in the number of ribbon contacts (Bartoletti et al., 2010), and the slightly smaller size of PSCs was likely due to the presence of fewer ribbon contacts in this sample, which we estimated from the peak PSC amplitude (91.1 pA/46 pA per ribbon contact) to be 1.98 ribbon contacts per pair. Consistent with this smaller amplitude simply reflecting a smaller number of ribbon contacts in this sample, using this number of ribbon contacts, the amplitude of the fast component of PSC charge transfer (559 fC) yielded an RRP of 18.2 vesicles/ribbon (Table I), similar to the RRP measured with 5 m*M* EGTA. In addition, the *y*-intercept of a straight line fit to the cumulative increase in charge transfer between 1 and 2 s during a train of −19 mV pulses (2450 fC) yielded a pool size of 80 vesicles/ribbon (Table I), similar to measurements made with 5 m*M* EGTA as the principal buffer. Allowing a greater spread of Ca^{2+} did not therefore appear to increase either PSC amplitude or maximum predicted pool sizes obtained with strong depolarizing steps. Weak Ca^{2+} buffering also did not stimulate greater additional release when using weaker depolarizing steps to −39 or −29 mV. Similar to results with 5 m*M* EGTA, both PSC amplitude and *y*-intercept values from the cumulative charge transfer plots declined in parallel with decreases in I_{Ca} evoked by different voltage steps (Fig. 4B). The finding that no additional vesicles were released despite a greater spread of Ca^{2+} with low buffering is consistent with earlier findings that release is controlled

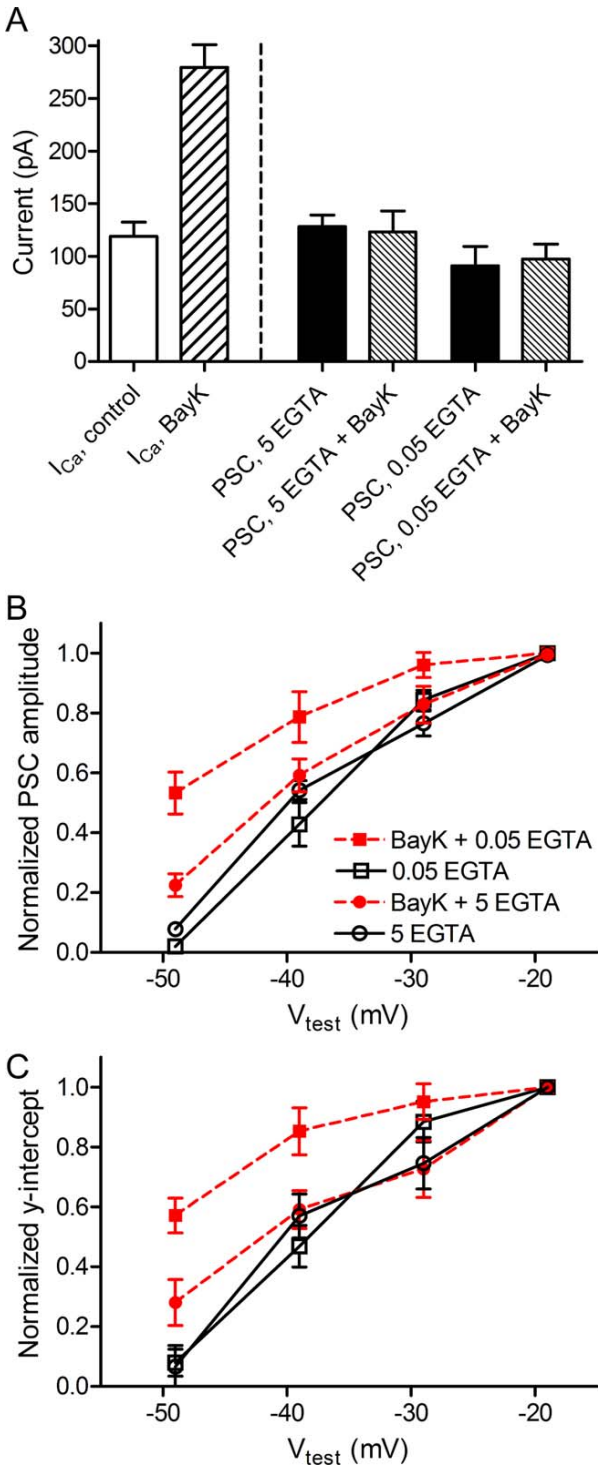

Fig. 4. Effects of BayK8644 and reduced Ca^{2+} buffering on PSCs. A: Bars at the left show the peak amplitude of I_{Ca} in control conditions and following application of 5 μ*M* BayK8644. 5 m*M* EGTA was used as the Ca^{2+} buffer in measurements of I_{Ca}. Bars at the right show that PSC amplitude evoked by a step to −19 mV did not differ significantly whether the cone pipette solution contained 5 m*M* or 0.05 m*M* EGTA as the principal Ca^{2+} buffer nor did they differ with addition of BayK8644 to the bathing solution (ANOVA, $p = 0.27$). Measurements of PSC amplitude (B) and *y*-intercept values from cumulative charge transfer plots (C) showed a similar voltage-dependent increase whether 0.05 (open squares) or 5 m*M* EGTA (open circles) was used as the principal Ca^{2+} buffer. Values were normalized to those at −19 mV. Application of BayK8644 increased PSC amplitude and *y*-intercept values at −49 mV but not other test potentials when using 5 m*M* EGTA. When using 0.05 m*M* EGTA, BayK8644 increased PSC amplitude and *y*-intercept values at −49, −39, and −29 mV.

by highly localized nanodomains of Ca^{2+} close to Ca^{2+} channels (Mercer et al., 2011).

Another way to increase the spread of Ca^{2+} is to increase its influx. We, therefore, tested effects of increasing I_{Ca} by bath application of the dihydropyridine agonist BayK8644 (5 μM). Use of BayK8644 more than doubled the peak amplitude of the L-type I_{Ca} in cones, increasing it from 119.2 ± 13.4 pA in control conditions ($n = 22$) to 279.6 ± 21.8 pA ($n = 10$; Fig. 4A). Despite this substantial increase in I_{Ca}, PSCs evoked by steps to −19 mV in BayK8644 (5 μM) were not significantly larger than control PSCs (Fig. 4A) whether using 5 or 0.05 mM EGTA as the intracellular buffer (BayK8644 + 5 mM EGTA, 123.1 ± 19.8, $n = 9$; BayK8644 + 0.05 mM EGTA, 94.7 ± 14.4, $n = 6$; comparison between all four groups by one-way ANOVA, $P = 0.27$; Fig. 4A). The maximum pool sizes obtained from the y-intercept of charge transfer measurements using steps to −19 mV were also similar to control conditions (BayK8644 + 5 mM EGTA, 3105 fC or 75 vesicles/ribbon; BayK8644 + 0.05 mM EGTA, 2190 fC or 69 vesicles/ribbon). The finding that PSCs evoked by steps to −19 mV were not increased by weaker intracellular Ca^{2+} buffering or by BayK8644-induced increases in I_{Ca} shows that there is a fixed upper limit to pool size and confirms earlier findings that maximal activation of I_{Ca} with a 25 ms step to −19 mV stimulates release of the entire RRP with a probability of 1 (Bartoletti et al., 2010).

When using 5 mM EGTA as the principal intracellular Ca^{2+} buffer in cones, PSC amplitude (Fig. 4B and 4C) and y-intercept (Fig. 4C) values measured in BayK8644 declined in a similar fashion as in control cells with use of weaker stimuli over most of the tested voltage range (−19 to −29 to −39 mV). It was only when using steps to −49 mV that we observed slightly larger PSC amplitude and y-intercept values with BayK8644 (Fig. 4B and 4C). These data are consistent with nanodomain regulation of release over much of the tested voltage range, with little overlap between the Ca^{2+} domains that control release of adjacent vesicles in the releasable pool, even when Ca^{2+} channel openings were lengthened substantially by application of BayK8644.

With use of 0.05 mM EGTA as the principal Ca^{2+} buffer in cones, the PSC amplitude and y-intercept values increased with weaker steps to −49, −39, and −29 mV (Fig. 4B and 4C). Thus, weak endogenous levels of Ca^{2+} buffering could be overwhelmed by the enhanced Ca^{2+} influx in BayK8644, stimulating release of a larger fraction of the releasable pool. Under these conditions, with weak Ca^{2+} buffering and exaggerated Ca^{2+} influx, the increased spread of Ca^{2+} was able to access a larger fraction of the releasable pool suggesting a transition from nanodomain to microdomain control of release. However, the maximum PSC amplitude and y-intercept values evoked by steps to −19 mV were still not larger than control values showing that the enhanced spread of Ca^{2+} did not expand the total available pool. This suggests an upper limit to the available pool size and a release probability of 1 with strong stimulation.

Measuring release and replenishment kinetics

Using the y-intercept value of cumulative increases in release to extrapolate the original available pool size during a train of pulses rests on assumptions that the number of release sites and the rate of replenishment remain constant. With maintained weak stimulation that does not fully activate I_{Ca}, the vesicle pool is not progressively depleted until empty but rather achieves a steady occupancy state after it is only partially depleted (Babai et al., 2010; Oesch and Diamond, 2011). Because the total pool is not completely emptied, the standard methods cannot be used to measure the total available pool size with less than maximal stimuli. In addition, different strength stimuli produce differences in intracellular Ca^{2+} levels that can alter the fraction of release sites available for rapid replenishment (Van Hook et al., 2014). Therefore, to calculate the total vesicle pool that is available for release with different strength stimuli, we developed an analytical model of release and replenishment that accounts for the history of release and incorporates measured properties of release and replenishment.

As illustrated in Figure 3A, the release of glutamate at the cone synapse proceeds with two kinetic components (Rabl et al., 2005), and, so, charge transfer during the PSC can be fit with a dual exponential function. With steps to −19 mV, the fast component of PSC charge transfer, which reflects release of the RRP, rose with a time constant of 5.2 ± 0.23 ms (Fig. 3A). The release time constant measured from PSC charge transfer is slightly longer than the release time constant measured from exocytotic capacitance jumps using test steps of varying duration ($\tau_r = 2.4$–2.7 ms; Rabl et al., 2005). This is because capacitance jumps measure the fusion of vesicles with the presynaptic plasma membrane whereas PSC charge transfer measurements also include the rise time kinetics of individual miniature PSCs, which reflect glutamate diffusion and binding to postsynaptic receptors. The second time constant for release is too long to be measured accurately with the brief 25-ms test pulses employed in these experiments (τ = 600–1400 ms; Bartoletti et al., 2010; Rabl et al., 2005).

Recovery from paired pulse depression at the cone synapse is almost entirely due to vesicle replenishment (Rabl et al., 2006), and, so, vesicle replenishment kinetics can be measured empirically by using paired pulse protocols and varying the interpulse interval. Van Hook et al. (2014) found that with steps

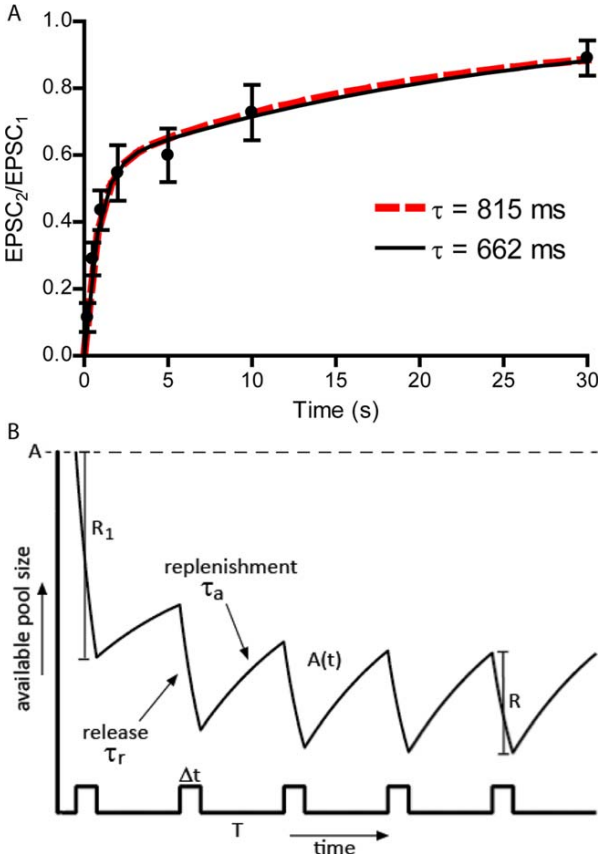

Fig. 5. A: Measurements of recovery from paired pulse depression with test steps to −39 mV (100 ms) at different interpulse intervals. PSCs recovered with time constants averaging $\tau_{fast} = 662$ ms and $\tau_{slow} = 19$ s and the fast time constant accounted for 52% of the recovery (black line). Fitting the same data with $\tau_{fast} = 816$ ms and $\tau_{slow} = 13$ s did not significantly alter the goodness of fit (dashed red line; $r^2 = 0.621$; $P = 0.6$, *F*-test). B: Illustration of the model. The initial stimulus during the pulse train triggers release of a number of vesicles, R_1, from the maximum available pool with size A. Release proceeds during the pulse of duration Δt at an exponential rate with a time constant of τ_r. During the interstimulus interval of duration T, the available pool of vesicles $A(t)$ is replenished at an exponential rate with time constant of τ_a. The limiting rate of release R is attained after achieving a steady state balance between release and replenishment.

to −19 mV, PSCs recovered from paired pulse depression with two time constants: $\tau_{fast} = 815$ ms and $\tau_{slow} = 13$ s (data from Van Hook et al., 2014). With this stimulus protocol, the fast time constant accounted for 76% of the recovery. Contributions from the faster component are enhanced by intracellular Ca^{2+} (Babai et al., 2010; Van Hook et al., 2014), and, so, we also measured replenishment kinetics with paired pulse protocols using weaker depolarizing steps to −39 mV (100 ms). With this weaker stimulus, PSCs exhibited bi-exponential recovery ($\tau_{fast} = 663$ ms, $\tau_{slow} = 19$ s; solid black line, filled circles, Fig. 5A), but the fast time constant accounted for a smaller fraction of recovery (52%) than with steps to −19 mV. If we fit the −39 mV data by constraining τ_{fast} to 815 ms, the contribution from the fast component increased slightly to 55% but fit quality did not differ significantly ($P = 0.55$; *F*-test; dashed red line, Fig. 5A). These results support previous evidence that changes in intracellular Ca^{2+} in cones act mainly to change the weighting of fast and slow components of replenishment but have little effect on the values of the individual time constants (Van Hook et al., 2014). For purposes of the present model, we assumed that the only effect of different voltage steps (to −39 and −19 mV) was to alter the proportion of vesicles subject to fast replenishment with a time constant of $\tau_a = 815$ ms. We varied the fraction of vesicles (f) that that contribute to fast replenishment from 76% for steps to −19 mV ($f_{-19} = 0.76$) to 55% for steps to −39 mV ($f_{-39} = 0.55$). Intervals between pulses were much shorter than the slow time constant of 13–19 s; so, we omitted the second time constant from the model.

Modeling release dynamics. The general features of the model are diagrammed in Figure 5B. On each test pulse, the release dynamics are governed by

$$\frac{dc}{dt} = \frac{p_s(A_i - c)}{\tau_r}$$

where $c = c(t)$ is the cumulative release from the beginning of the pulse and A_i the available pool size at the start of the ith pulse. The timescale, τ_r regulates release during strong pulses (steps to −19 mV) and is made effectively slower for weaker stimuli (steps to −39 mV) by a smaller stimulus-dependent release factor, p_s, with $0 < p_s \leq 1$. Note that $p_s = 1$ for strong pulses, since τ_r is the measured release timescale for strong pulses.

Solving this differential equation yields

$$c(t) = A_i\left(1 - e^{\frac{-p_s t}{\tau_r}}\right)$$

The total release during a stimulus pulse of length Δt is thus $R_i = c(\Delta t)$, giving

$$R_i = P_s A_i \text{ where } P_s = 1 - e^{\frac{-p_s \Delta t}{\tau_r}}$$

is the stimulus-dependent release probability for a pulse of length Δt. With τ_r = 5 ms and $\Delta t = 25$ ms, this formula predicts that strong test pulses (steps to −19 mV) have release probability $P_{-19} = 1 - e^{-5} = 0.9933$. For τ_r = 2.4 ms, release probability is even closer to 1. These predictions are consistent with results from BayK8644 experiments described earlier and previous work showing that 25 ms steps to −19 mV evoke release with a probability of 1 (Bartoletti et al., 2010).

Replenishment dynamics. The model accounts for the number of available release sites (i.e., occupancy

state of the releasable pool) by assuming that replenishment occurs at a rate proportional to the number of empty sites available for occupancy by new vesicles. This assumption is supported by evidence that vesicle replenishment rates measured with strong steps that empty the RRP vary linearly with the size of the RRP (Babai et al., 2010). We assume that replenishment during the stimulus pulse is small compared with the interpulse period. The replenishment between pulses can be described by:

$$\frac{da}{dt}=\frac{(n-a)}{\tau_a}$$

where $a = a(t)$ is the cumulative replenishment t seconds from the end of the previous pulse, n the initial number of sites on the ribbon available for replenishment, and τ_a the replenishment time constant. Solving this equation and evaluating at time T, the length of the interpulse intervals, yields a total replenishment:

$$a(T)=n\left(1-e^{\frac{-T}{\tau_a}}\right)=n(1-\beta)$$

where $\beta = e^{\frac{-T}{\tau_a}}$ is a dimensionless replenishment factor.

Estimate of maximum available pool size A_s. We find (see supporting calculations) that we can estimate the maximum available pool size A_s from the limiting release R_s as

$$A_s=\left[\frac{1}{P_s}+\frac{\beta}{1-\beta}\right]\frac{R_s}{f_s}$$

where f_s is the stimulus-dependent fraction of fast-replenishing ribbon sites. Recall that, for strong stimuli, $P_{-19} \approx 1$. This immediately allows us to estimate the maximum available pool size as

$$A_{-19}=\frac{R_{-19}}{(1-\beta)f_{-19}}$$

Using the values $f_{-19} = 0.76$, $\tau_a = 815$ ms, and $T = 50$ ms, we obtain $\beta = 0.94$ and $A_{-19} = 22.2\ R_{-19}$. For a longer interpulse interval of $T = 125$ ms, we obtain $\beta = 0.86$ and $A_{-19} = 9.3\ R_{-19}$.

For other stimuli, such as steps to −39 mV, we can use measurements of the amount of release evoked by the first pulse, $(R_1)_s$, to replace P_s and obtain a closed form expression for the maximum available pool size (see supporting calculations):

$$A_s=\frac{\beta}{(1-\beta)}\frac{R_s(R_1)_s}{\left(f_s(R_1)_s-R_s\right)} \quad (1)$$

We can easily check that, for the strong stimulus, assuming $P_{-19}=1$ so that $(R_1)_{-19}=A_{-19}$, we recover from this equation our previous expression for A_{-19}.

Finally, the release probability P_s can be estimated using $P_s=(R_1)_s/A_s$:

$$P_s=\frac{(1-\beta)}{\beta}\frac{\left(f_s(R_1)_s-R_s\right)}{R_s}$$

Again, we can check that for strong stimuli, using the fact that $(R_1)_{-19}=A_{-19}= R_{-19}/(1-\beta)f_{-19}$, we recover $P_{-19}=1$.

Results of the model: To implement the model, we determined the limiting release value, R, from the cumulative increase in amplitude occurring 1–2 s into the pulse trains ($T = 50$ ms, 5 mM EGTA buffer) shown in Figure 2. With a train of steps to −19 mV (25 ms), the model predicted that release of the entire releasable pool should generate a PSC of 131.3 pA (Table I), nearly the same size as the actual PSC evoked by the initial step in the pulse train [$(R_1)_{-19} = 128$ pA]. With a train of steps to −39 mV (25 ms, Fig. 2), Eq. (1) predicted a nearly identical pool size yielding a maximal PSC of 131.2 pA ($A_{-39}/A_{-19} = 1.0$, Table I). This in turn predicts that the release probability attained during a step to −39 mV was 70.9 pA/131.2 pA or 0.54. The pool sizes estimated from the y-intercept values of cumulative release plots in Figure 2 suggested a pool size of 137 pA for the −19 mV pulse train and a pool of 74 pA for the −39 mV pulse train ($A_{-39}/A_{-19} = 0.54$). These data suggest that the smaller pool of vesicles emptied by the weaker stimulus reflects a lower release probability that empties a smaller fraction of the total pool.

A key feature of the model is the incorporation of vesicle replenishment between test pulses. We, therefore, tested the model with data from a different set of cone/HC pairs using a longer interpulse interval ($T = 125$ ms), but with the same test pulse duration of 25 ms. Using the values of R_{-19} and R_{-39} obtained from cumulative amplitude measurements ($n = 6$), Eq. (1) of the model predicted pool sizes yielding PSCs of 137 and 131 pA for −19 and −39 mV steps, respectively, nearly identical to one another ($A_{-39}/A_{-19} = 0.96$, Table I). The fast component of the PSC charge transfer in this sample of cell pairs averaged 774 fC, suggesting an RRP of 16.8 vesicles/ribbon (Table I). The y-intercept of a straight line fit to the cumulative increase in charge transfer between 1 and 2 s during a train of −19 mV pulses (3214 fC) yielded a pool size of 70 vesicles/ribbon (Table I).

We next tested the model using the pulse train data obtained with 0.05 mM EGTA as the principal Ca^{2+} buffer in the cone patch pipette (data from Fig. 4). Once again, the model predicted equal pool sizes with steps to −19 and −39 mV of 111 and 114 pA, respectively ($A_{-39}/A_{-19} = 1.02$; Table I). The model predicted a pool size yielding an initial PSC

amplitude of 110 pA, somewhat larger than the actual PSC evoked by a step to −19 mV of 91 pA. However, replenishment is Ca^{2+}-dependent and is, therefore, accelerated by lowering intracellular Ca^{2+} buffering in cones (Babai et al., 2010). We estimated the impact of weaker intracellular Ca^{2+} buffering on replenishment kinetics by measuring recovery from paired pulse depression (25 ms steps to −19 mV) following a 2-s interval. In that time, PSCs recovered by $66.6 \pm 6.5\%$ ($n = 9$) with 5 m*M* EGTA in the cone pipette solution and by $70.4 \pm 6.5\%$ ($n = 8$) with 0.05 m*M* EGTA. A 5% increase in recovery after 2 s can be explained by a 6.5% increase in the contribution from fast replenishment. Increasing the fraction of fast replenishing sites by 6.5% increased the predicted pool sizes to 102.9 and 99.8 pA for steps to −19 and −39 mV, respectively, closer to the actual PSC amplitude of 91 pA evoked by steps to −19 mV.

We tested our model at another synapse by asking whether it could predict vesicle pool sizes using published values from the calyx of Held in juvenile rats (P8–P10). We used a fast replenishment time constant of $\tau_a = 196$ ms with the fraction of replenishment mediated by the fast component $f = 0.49$ (Sakaba and Neher, 2001). For the limiting rate of release R_s, we measured the cumulative increase in PSC amplitude evoked by trains of action potentials (100 Hz) in 2 mM Ca^{2+} from Figure 4 of Schneggenburger et al. (1999) to obtain $R_s = 0.32$ nA/action potential. For Δt we used the action potential half-width of 0.55 ms from the same study (Schneggenburger et al., 1999). With these values, the model predicted a pool size of 15.0 nA or 522 vesicles. By comparison, using the back-extrapolation method, Schneggenburger et al. (1999) concluded that the pool size was ∼600 vesicles. Taschenberger et al. (2002) found a larger pool size of ∼2000 quanta in P12–P14 rats. In their experiments, the limiting slope of the cumulative increase in PSC amplitude evoked by a train of action potentials (100 Hz) in 2 m*M* Ca^{2+} was $R_s = 2.2$ nA/action potential (Fig. 8 from Taschenberger et al., 2002). The action potential half-width in rats of this age was 0.21 ms (Taschenberger et al., 2002). Using the same properties of replenishment as before ($\tau_a = 196$ ms and $f = 0.49$), the model predicted a pool of 4046 vesicles. However, the fraction of vesicles *f* undergoing fast replenishment at the calyx of Held has been found to be as great as 0.71 (Guo et al., 2015). Using this larger value for *f*, the model yielded a pool of 2139 vesicles, in close agreement with the pool size found by Taschenberger et al. (2002). In addition to showing that the model can be applied to conventional synapses, these results emphasize the sensitivity of pool size estimates to replenishment rates and specifically the fraction, *f*, of vesicles undergoing fast replenishment.

DISCUSSION

In this study, we developed an analytical model of release and replenishment that allowed us to compare vesicle pool sizes emptied by weak and strong stimulation. We found that weak and strong depolarizing voltage steps emptied vesicles from a releasable pool of the same size at the cone ribbon synapse. Enhancing the spread of Ca^{2+} within cone terminals by lowering intracellular Ca^{2+} buffering to 0.05 m*M* EGTA or by increasing Ca^{2+} influx with application of the dihydropyridine agonist BayK8644 did not increase the maximum pool size, consistent with a release probability of 1 when cones are strongly depolarized (Bartoletti et al., 2010). The fact that enhancing the spread of Ca^{2+} to nonribbon sites with use of low Ca^{2+} buffering and BayK8644 did not amplify release also substantiates the conclusion that release at cones occurs only at synaptic ribbons (Snellman et al., 2011). Interestingly, rods operate differently from cones with a substantial fraction of release occurring at nonribbon sites (Chen et al., 2013, 2014).

By accounting for release site occupancy and measured properties of replenishment, the analytical model developed in this study allowed us to compare the total available vesicle pools under various stimulus conditions where the rate of replenishment and number of release sites available for replenishment differed considerably. The measurements needed to predict pool size with this formula are the rate of replenishment, the size of the initial PSC, the amount of release evoked per pulse after achieving steady state, and the fraction of release sites subject to rapid replenishment (*f*). The predictions of the model are particularly sensitive to measurements of the release per pulse, kinetics of replenishment, and *f*. This was emphasized by analyzing published data from the calyx of Held. The formula that we derived predicted a vesicle pool size at the calyx of Held of ∼520 vesicles, similar to that found by Schneggenburger et al. (1999) in P8–P10 rats. In studies on P10–P14 rats, Taschenberger et al. (2002) reported nearly 10-fold more release per pulse and the model thus predicted a nearly 10-fold larger pool size of ∼4000 vesicles. This is roughly twice as large as the pool size determined by Taschenberger et al. (2002) but we found a pool of ∼2000 vesicles if we used a value for *f* found by Guo et al. (2015) of 0.71 in place of 0.49 found by Sakaba and Neher (2001). The model incorporated Ca^{2+}- and voltage-dependent changes to *f* that are known to occur at the cone synapse (Van Hook et al., 2014), but these changes may not be present at every synapse. This aspect of the model can easily be ignored by using the same value of *f* for different stimulus conditions. Replenishment rates can vary substantially among synapses, and this will also have an important impact on the model predictions. For example, frog auditory

hair cell ribbon synapses show more rapid replenishment than cone ribbon synapses with time constants of 84 ms and 2.9 s (Cho et al., 2011). The model incorporated only the fast time constant for replenishment. To analyze data from cells with rapid second time constants or with longer interpulse intervals, one would need to incorporate slower components of replenishment.

The results of this study indicate that vesicle pool size at the cone ribbon synapse remains fixed—at least over a time scale of minutes—although it may change over longer periods. For example, photoreceptor ribbons are capable of assembling and disassembling on a daily basis (Abe and Yamamoto, 1984; Adly et al., 1999; Balkema et al., 2001), perhaps in response to changing NAD/NADH levels (Magupalli et al., 2008). Changes in vesicular glutamate levels, vesicle diameter, and postsynaptic receptor composition also produce only slow changes in quantal amplitude (Bartoletti and Thoreson, 2011; Ishikawa et al., 2002; Karunanithi et al., 2002; Wilson et al., 2005; see Ariel and Ryan, 2012 for review). However, given that quantal amplitude (Q) and pool size (N) remain relatively fixed over shorter periods, our results indicate that rapid light-evoked changes in cone membrane potential are encoded into postsynaptic responses entirely by changes in release probability (P). This in turn suggests that, like bipolar cell ribbon synapses (Oesch and Diamond, 2011), changes in luminance that alter the cone membrane potential are encoded entirely by changes in occupancy of a single, fixed-size RRP.

The size of the RRP suggested by cumulative amplitude measurements matched the amplitude of the PSC evoked by a step to −19 mV. Thus, a strong pulse empties the RRP with a release probability of 1. Dividing this PSC amplitude by the average mEPSC quantal amplitude in salamander HCs of 5.7 pA (Cadetti et al., 2008) suggests that the peak of the PSC results from the concerted actions of 8–10 vesicles/ribbon. However, we believe this to be an underestimate of the total RRP because, even during fast release, not all vesicles in the RRP are released simultaneously. Integrating charge transfer during the PSC allows one to count all of the vesicles that were released (Cadetti et al., 2005, 2008). To measure the entire RRP, we therefore measured the fast component of the increase in PSC charge transfer evoked by a step to −19 mV and found that it averaged 17–18 vesicles/ribbon (Table I). The releasable pool depleted during sustained stimulation at the calyx of Held matches the RRP (Schneggenburger et al., 2002). From cumulative amplitude measurements, we conclude that the entire RRP was released by the first pulse in a strong pulse train (25 ms pulses to −19 mV). Although a strong test pulse applied to a cone (25 ms pulses to −19 mV) emptied the entire RRP, from the y-intercept values of cumulative charge transfer plots, we found that the total pool emptied during a train of strong pulses exceeded the RRP and consisted of 64–80 vesicles (Table I). This release of additional vesicles was not evident in the cumulative amplitude plots, which measure only synchronized release of vesicles, but was seen only in charge transfer measurements, which include both synchronous and synchronous release. This suggests that much of this additional release was asynchronous. Depolarization-evoked release at cone synapses appears to occur entirely at ribbons (Snellman et al., 2011; Van Hook and Thoreson, 2015), and, so, these additional 46–63 vesicles likely represent a ribbon-related reserve pool that is 3–4 times larger than the RRP. This is similar to primate foveal cones where ultrastructural studies show about four times as many vesicles at ribbon reserve sites as found in the anatomically defined RRP of vesicles at the base of the ribbon (Sterling and Matthews, 2005). We found that the maximum pool size was not increased by lowering intracellular Ca^{2+} buffering or by use of BayK8644 indicating that this pool could not be expanded by increasing the spread of Ca^{2+} up the ribbon or into surrounding perisynaptic regions. Jackman et al. (2009) showed that delivery of vesicles to ribbon release sites, not fusion, was the rate-limiting step in sustained release. They proposed that this was due to slow delivery of vesicles down the ribbon to release sites. However, the present evidence that the size of the total releasable pool is similar to the number of vesicles on the ribbon is more consistent the hypothesis that the rate-limiting step in vesicle delivery is not descent of vesicles down the ribbon but rather attachment of vesicles to the ribbon (Van Hook et al., 2014).

The conclusion that changes in cone membrane potential are encoded into postsynaptic responses solely by changes in release probability suggests a direct relationship between Ca^{2+} channel open probability and vesicle release. Previous calculations indicate that there are 56–80 Ca^{2+} channels clustered beneath each ribbon in salamander cones (Bartoletti, et al., 2011), which in turn suggests there are three to five channels associated with each vesicle in the RRP, identical to conclusions at hippocampal synapses (Bucurenciu et al., 2010). The peak Ca^{2+} channel open probability attained with steps to −19 mV approaches ~0.3 in cones (Bartoletti et al., 2011), suggesting that only one or two channels per vesicle are likely to be open at any instant. The ability of the entire RRP to be released by a step to −19 mV is therefore consistent with earlier evidence that fusion of a single vesicle at the cone synapse can be triggered by opening of only one to three Ca^{2+} channels (Bartoletti et al, 2011), much like a number of other synapses (Brandt et al., 2005; Bucurenciu et al.,

2010; Graydon et al., 2011; Jarsky et al., 2010; Stanley, 1993; reviewed by Eggermann et al. 2011). Given that changes in PSC amplitude arise solely from changes in release probability, then the number of channels at the cone synapse appears optimized to provide just enough Ca^{2+} to trigger rapid release of all of the vesicles in the RRP when I_{Ca} is fully activated. By activating fewer channels, weaker depolarization would stimulate release of smaller fraction of the RRP. This sensitive nanodomain control of release produces changes in release probability that vary linearly with the number of open channels. If there were an excess number of channels beneath each release site, then reducing the number of open channels by weaker activation of I_{Ca} would not reduce release probability. This is similar to experiments in which we applied BayK8644 to increase Ca^{2+} channel open probability while using 0.05 m*M* EGTA to mimic endogenous Ca^{2+} buffering conditions. In these experiments, PSC amplitude did not decline when the step depolarization was reduced from −19 to −29 mV. Ribbons can vary in size from one another, and we predict that the number of channels beneath each ribbon will vary with the size of the ribbon and the number of vesicles in the RRP. Similar to other neuronal properties, optimization of vesicle pool size and Ca^{2+} channel number was driven by evolutionary pressures balancing competing requirements for maximizing information transfer while minimizing energy consumption (Sterling, 2013).

SUPPORTING CALCULATIONS

At the start of each stimulus pulse, the available pool size A_i is equal to the pool size at the end of the previous pulse, $A_{i-1}(1-P_s)$, plus the amount of replenishment between pulses, $a(T)= n(1- \beta)$. Here, n is the quantity of ribbon sites available for replenishment at the end of the previous pulse:

$$n=f_sA_s-A_{i-1}(1-P_s).$$

This is the total number of fast-replenishing sites, f_sA_s, minus the remaining pool size at the end of the previous pulse. In particular, $a(T)=[f_sA_s-A_{i-1}(1-P_s)](1-\beta)$, and

$$A_i=A_{i-1}(1-P_s)+a(T)=f_sA_s(1-\beta)+\beta(1-P_s)A_{i-1}.$$

Letting $b=\beta(1-P_s)$ and $c=f_sA_s(1-\beta)$, this is a recursion relation for the sequence of pool sizes $\{A_i\}$ of the form $A_i=bA_{i-1}+c$. We can solve this recursion relation using ordinary generating functions to obtain an explicit formula for the pool sizes at the start of each stimulus pulse:

$$A_i= A_1b^{i-1}+c\left(\frac{1-b^{i-1}}{1-b}\right)$$

where $A_1=A_s$ is the total available pool size preceding the first pulse. Taking the limit as $i\to\infty$ yields $A_\infty=\frac{c}{1-b}$, giving a limiting value of

$$A_\infty=\frac{f_sA_s(1-\beta)}{1-\beta+\beta P_s}$$

Since the release on each stimulus pulse is given by $R_i=P_sA_i$, the limiting release is

$$R_s=P_sA_\infty=\frac{f_sP_sA_s(1-\beta)}{1-\beta+\beta P_s}.$$

This allows us to solve for the maximum available pool size in terms of P_s, R_s, and f_s:

$$A_s=\frac{\left[\frac{1}{P_s}+\frac{\beta}{1-\beta}\right]R_s}{f_s}$$

Next, assuming that $A_1=A_s$, so that the maximum pool size is available on the very first stimulus pulse, we have $(R_1)_s=P_sA_s$; so that

$$P_s=\frac{(R_1)_s}{A_s}$$

Plugging this into the above expression for A_s yields

$$A_s=\frac{\left[\frac{A_s}{(R_1)_s}+\frac{\beta}{1-\beta}\right]R_s}{f_s}$$

Now, we can solve for A_s explicitly in terms of $(R_1)_s$, R_s, and f_s:

$$A_s=\frac{\left(\frac{\beta}{1-\beta}\right)R_s(R_1)_s}{f_s(R_1)_s-R_s.}$$

REFERENCES

Abe H, Yamamoto TY. 1984. Diurnal changes in synaptic ribbons of rod cells of the turtle. J Ultrastruct Res 86:246–251.

Adly MA, Spiwoks-Becker I, Vollrath L. 1999. Ultrastructural changes of photoreceptor synaptic ribbons in relation to time of day and illumination. Invest Ophthalmol Vis Sci 40:2165–2172.

Ariel P, Ryan TA. 2012. New insights into molecular players involved in neurotransmitter release. Physiology (Bethesda) 27: 15–24.

Babai N, Bartoletti TM, Thoreson WB. 2010. Calcium regulates vesicle replenishment at the cone ribbon synapse. J Neurosci 30: 15866–15877.

Balkema GW, Cusick K, Nguyen TH. 2001. Diurnal variation in synaptic ribbon length and visual threshold. Vis Neurosci 18:789–797.

Bartoletti TB, Thoreson WB. 2011. Quantal amplitude at the cone ribbon synapse can be adjusted by changes in cytosolic glutamate. Mol Vis 17:920–931.

Bartoletti TM, Babai N, Thoreson WB. 2010. Vesicle pool size at the salamander cone ribbon synapse. J Neurophysiol 103:419–423.

Bartoletti TM, Jackman SL, Babai N, Mercer AJ, Kramer RH, Thoreson WB. 2011. Release from the cone ribbon synapse under

bright light conditions can be controlled by the opening of only a few Ca^{2+} channels. J Neurophysiol 106:2922–2935.
Brandt A, Khimich D, Moser T. 2005. Few $Ca_V1.3$ channels regulate the exocytosis of a synaptic vesicle at the hair cell ribbon synapse. J Neurosci 25:11577–11585.
Bucurenciu I, Bischofberger J, Jonas P. 2010. A small number of open Ca^{2+} channels trigger transmitter release at a central GABAergic synapse. Nat Neurosci 13:19–21.
Cadetti L, Tranchina D, Thoreson WB. 2005. A comparison of release kinetics and glutamate receptor properties in shaping rod-cone differences in EPSC kinetics in the salamander retina. J Physiol 569:773–788.
Cadetti L, Bartoletti TM, Thoreson WB. 2008. Quantal mEPSCs and residual glutamate: how horizontal cell responses are shaped at the photoreceptor ribbon synapse. Eur J Neurosci 27:2575–2586.
Chen M, Van Hook MJ, Zenisek D, Thoreson WB. 2013. Properties of ribbon and non-ribbon release from rod photoreceptors revealed by visualizing individual synaptic vesicles. J Neurosci 33:2071–2086.
Chen M, Križaj D, Thoreson WB. 2014. Intracellular calcium stores drive slow non-ribbon vesicle release from rod photoreceptors. Front Cell Neurosci 8:20.
Cho S, Li GL, von Gersdorff H. 2011. Recovery from short-term depression and facilitation is ultrafast and Ca^{2+} dependent at auditory hair cell synapses. J Neurosci 31:5682–5692.
Christensen BN, Martin AR. 1970. Estimates of probability of transmitter release at the mammalian neuromuscular junction. J Physiol 210:933–945.
del Castillo J, Katz B. 1954. Quantal components of the end-plate potential. J Physiol 124:560–573.
Eggermann E, Bucurenciu I, Goswami SP, Jonas P. 2011. Nanodomain coupling between Ca^{2+} channels and sensors of exocytosis at fast mammalian synapses. Nat Rev Neurosci 13:7–21.
Elmqvist D, Quastel DM. 1965. A quantitative study of end-plate potentials in isolated human muscle. J Physiol 178:505–529.
Furukawa T, Matsuura S. 1978. Adaptive rundown of excitatory post-synaptic potentials at synapses between hair cells and eight nerve fibres in the goldfish. J Physiol 276:193–209.
Gomis A, Burrone J, Lagnado L. 1999. Two actions of calcium regulate the supply of releasable vesicles at the ribbon synapse of retinal bipolar cells. J Neurosci 19:6309–6317.
Graydon CW, Cho S, Li GL, Kachar B, von Gersdorff H. 2011. Sharp Ca^{2+} nanodomains beneath the ribbon promote highly synchronous multivesicular release at hair cell synapses. J Neurosci 31:16637–16650.
Guo J, Ge JL, Hao M, Sun ZC, Wu XS, Zhu JB, Wang W, Yao PT, Lin W, Xue L. 2015. A three-pool model dissecting readily releasable pool replenishment at the calyx of held. Sci Rep 5:9517.
Ishikawa T, Sahara Y, Takahashi T. 2002. A single packet of transmitter does not saturate postsynaptic glutamate receptors. Neuron 34:613–621.
Jackman S, Choi S-Y, Thoreson WB, Rabl K, Bartoletti TM, Kramer RH. 2009. Role of the synaptic ribbon in transmitting the cone light response. Nat Neurosci 12:303–310.
Jarsky T, Tian M, Singer JH. 2010. Nanodomain control of exocytosis is responsible for the signaling capability of a retinal ribbon synapse. J Neurosci 30:11885–11895.
Karunanithi S, Marin L, Wong K, Atwood HL. 2002. Quantal size and variation determined by vesicle size in normal and mutant Drosophila glutamatergic synapses. J Neurosci 22:10267–10276.
Magupalli VG, Schwarz K, Alpadi K, Natarajan S, Seigel GM, Schmitz F. 2008. Multiple RIBEYE-RIBEYE interactions create a dynamic scaffold for the formation of synaptic ribbons. J Neurosci 28:7954–7967.
Mercer AJ, Rabl K, Riccardi GE, Brecha NC, Stella SL Jr, Thoreson WB. 2011. Location of release sites and calcium-activated chloride channels relative to calcium channels at the photoreceptor ribbon synapse. J Neurophysiol 105:321–335.
Oesch NW, Diamond JS. 2011. Ribbon synapses compute temporal contrast and encode luminance in retinal rod bipolar cells. Nat Neurosci 14:1555–1561.
Pang JJ, Gao F, Barrow A, Jacoby RA, Wu SM. 2008. How do tonic glutamatergic synapses evade receptor desensitization? J Physiol 586:2889–2902.
Rabl K, Cadetti L, Thoreson WB. 2005. Kinetics of exocytosis is faster in cones than in rods. J Neurosci 25:4633–4640.
Rabl K, Cadetti L, Thoreson WB. 2006. Paired-pulse depression at photoreceptor synapses. J Neurosci 26:2555–2563.
Ruiz R, Cano R, Casañas JJ, Gaffield MA, Betz WJ, Tabares L. 2011. Active zones and the readily releasable pool of synaptic vesicles at the neuromuscular junction of the mouse. J Neurosci 31:2000–2008.
Sakaba T, Neher E. 2001. Calmodulin mediates rapid recruitment of fast-releasing synaptic vesicles at a calyx-type synapse. Neuron 32:1119–1131.
Sakaba T, Schneggenburger R, Neher E. 2002. Estimation of quantal parameters at the calyx of Held synapse. Neurosci Res 44: 343–356.
Schneggenburger R, Meyer AC, Neher E. 1999. Released fraction and total size of a pool of immediately available transmitter quanta at a calyx synapse. Neuron 23:399–409.
Schneggenburger R, Sakaba T, Neher E. 2002. Vesicle pools and short-term synaptic depression: Lessons from a large synapse. Trends Neurosci 25:206–212.
Snellman J, Mehta B, Babai N, Bartoletti TM, Akmentin W, Francis A, Matthews G, Thoreson W, Zenisek D. 2011. Acute destruction of the synaptic ribbon reveals a role for the ribbon in vesicle priming. Nat Neurosci 14:1135–1141.
Stanley EF. 1993. Single calcium channels and acetylcholine release at a presynaptic nerve terminal. Neuron 11:1007–1011.
Sterling P. 2013. Some principles of retinal design: the Proctor lecture. Invest Ophthalmol Vis Sci 54:2267–2275.
Sterling P, Matthews G. 2005. Structure and function of ribbon synapses. Trends Neurosci 28:20–29.
Taschenberger H, Leão RM, Rowland KC, Spirou GA, von Gersdorff H. 2002. Optimizing synaptic architecture and efficiency for high-frequency transmission. Neuron 36:1127–1143.
Thanawala MS, Regehr WG. 2013. Presynaptic calcium influx controls neurotransmitter release in part by regulating the effective size of the readily releasable pool. J Neurosci. 33:4625–4633.
Thoreson WB, Tranchina D, Witkovsky P. 2003. Kinetics of synaptic transfer from rods and cones to horizontal cells in the salamander retina. Neuroscience 122:785–798.
Thoreson WB, Rabl K, Townes-Anderson E, Heidelberger R. 2004. A highly Ca^{2+}-sensitive pool of vesicles contributes to linearity at the rod photoreceptor ribbon synapse. Neuron 42:595–605.
Van Hook MJ, Thoreson WB. 2013. Simultaneous whole cell recordings from photoreceptors and second-order neurons in an amphibian retinal slice preparation. J Vis Exp 122:e50007.
Van Hook MJ, Thoreson WB. 2014. Endogenous calcium buffering at photoreceptor synaptic terminals in salamander retina. Synapse 68:518–528.
Van Hook MJ, Parmelee CM, Chen M, Cork KM, Curto C, Thoreson WB. 2014. Fast vesicle replenishment of the ribbon is mediated by calmodulin and shapes the filtering of synaptic transmission by cone photoreceptors. J Gen Physiol. 144:357–378.
Van Hook MJ, Thoreson WB. 2015. Weak endogenous Ca^{2+} buffering supports sustained synaptic transmission by distinct mechanisms in rod and cone photoreceptors in salamander retina. Physiol Rep 3:pii e12567.
von Gersdorff H, Vardi E, Matthews G, Sterling P. 1996. Evidence that vesicles on the synaptic ribbon of retinal bipolar neurons can be rapidly released. Neuron 16:1221–1227.
Wilson NR, Kang J, Hueske EV, Leung T, Varoqui H, Murnick JG, Erickson JD, Liu G. 2005. Presynaptic regulation of quantal size by the vesicular glutamate transporter VGLUT1. J Neurosci 25: 6221–6234.
Witkovsky P, Schmitz Y, Akopian A, Krizaj D, Tranchina D. 1997. Gain of rod to horizontal cell synaptic transfer: relation to glutamate release and a dihydropyridine-sensitive calcium current. J Neurosci 17:7297–7306.